Applications in Energy and Combustion Science 22 (2025) 100329

Contents lists available at ScienceDirect

Applications in Energy and Combustion Science

journal homepage: www.sciencedirect.com/journal/applications-in-energy-and-combustion-science

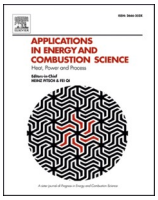

Applicability of Optical Emission Spectroscopy for Industrial Flame Analysis with Hydrogen and Natural Gas Mixtures Based on Laboratory Study

Arto Rautioaho [a,*], Henri Pauna [a], Mikko Jokinen [b], Oskari Seppälä [b], Elsa Busson [c], Lukas Sankowski [c], Ville-Valtteri Visuri [a], Timo Fabritius [a]

[a] Process Metallurgy Research Unit, P.O. Box 4300, 90014 University of Oulu, Finland
[b] Luxmet Oy, Paavo Havaksen tie 5 C, 90570 Oulu, Finland
[c] Department for Industrial Furnaces and Heat Engineering, RWTH Aachen University, Kopernikusstr. 10, 52074 Aachen, Germany

ARTICLE INFO

Keywords:
Flame analysis
Optical emission spectroscopy
Hydrogen combustion
Soot particles
Thermal radiation

ABSTRACT

This study investigates optical emission spectroscopy as an analysis method for hydrogen and natural gas burner flames relevant to industrial use. The equipment used was a low-cost industrial spectrometer, which measures light in the wavelength range of 500–1000 nm. Measurements were conducted with an open flame burner and a burner-heated furnace, with different mixture ratios of natural gas and hydrogen. Based on the results, it can be concluded that the relative amount of thermal radiation and soot particles from an open flame can be approximated using optical spectra. When adding hydrogen to a natural gas flame, the solid angle of soot particles rises by the first 5–16% of hydrogen, leading to higher thermal radiation. With higher shares of hydrogen, the solid angle of soot particles decreases radically, leading to lower thermal radiation. The temperatures that were measured from the optical spectra based on radiation from soot particles show that the flame's temperature could be measured up to 46% share of hydrogen. In the burner-heated furnace, the intensive thermal radiation from the inner walls gets mixed with the radiation from the flame, making it easier to determine the temperature of the wall rather than the flame itself. The study also presents the spectroscopic differences between different gas mixtures. In addition, the background phenomena and practical effects of these differences are discussed.

1. Introduction

Greenhouse gas emissions are one of the most significant challenges facing humanity today. Emissions must be cut in several sectors, with the steel industry being one of the largest emitters of greenhouse gases. The greenhouse gas emissions of the steel industry are related primarily to the use of fossil carbon-based reductants and burners operated with fossil fuels [1].

Burners are used, among others, as an auxiliary energy source in electric arc furnaces, and for ladle pre-heating at the melt shop, for slab reheating in the hot rolling mill, and for annealing in the cold rolling. Considering a shift to hydrogen burners in slab reheating and annealing furnaces, major research topics in the literature include changes in scale formation [2] and process control. Efficient control of the hydrogen burners necessitates efficient monitoring methods. Information on the combustion process is typically obtained via off-gas analysis, which, in non-closed spaces, is subject to inaccuracies due to leakage air. Direct information on the flame properties would enable more accurate adjustment of the burner's operating parameters.

Optical spectroscopy has had a significant role in the development of physics, chemistry, and astronomy [3,4], and spectroscopy has been used for flame analysis for over 200 years [5]. However, only the technical development of the last few decades has made inexpensive real-time analysis methods based on spectroscopy possible. Based on this background, optical emission spectroscopy (OES) has been envisioned as a potential solution for direct monitoring of flames in metallurgical furnaces [6]. The advantage of OES is the rapid measurement and simple and relatively low-cost equipment. OES provides information on, for example, temperature and composition. Over the last decade, OES has been successfully applied for monitoring electric arc furnaces [7] and ladle furnaces [8], highlighting the robustness of OES in high-temperature environments.

* Corresponding author.
E-mail address: arto.rautioaho@oulu.fi (A. Rautioaho).

https://doi.org/10.1016/j.jaecs.2025.100329
Received 23 January 2025; Received in revised form 27 February 2025; Accepted 8 March 2025
Available online 9 March 2025

This work aimed to study the applicability of OES for analyzing flames from industrially relevant burners operated with natural gas (NG), hydrogen gas (H_2), and their mixtures. More specifically, the study considers the 500–1000 nm wavelength range with different natural gas and hydrogen mixture ratios, focusing on flame temperature, heat radiation, and phenomena related to flame properties. The research aims to provide information on which situations OES is suitable for flame analysis and what the limitations of its use are. In addition, the study discusses the results of the measurements and the kind of observations about the properties of the flame that could be clarified with the OES method.

2. Materials and methods

2.1. Burners and furnace setup

Experiments were conducted at the Department for Industrial Furnaces and Heat Engineering at the RWTH Aachen University, Germany. The spectroscopic measurements were conducted with an open flame burner Kromschröder BIC 100HB-0/35-(37)E and a furnace with a multifuel burner prototype with different hydrogen and natural gas mixture ratios. The burners allowed power and air-fuel equivalence ratio (lambda value, i.e., used air-fuel ratio per stoichiometric air-fuel ratio) to be kept at the same level, and the ratios of fuel compositions were changed during the measurement session. During the measurements, the open flame burner's power was 15 kW (test 1) or 30 kW (test 2), and the power of the burner-heated furnace was 190 kW (test 3). The burner-heated furnace was equipped with eight temperature sensors (type N thermocouples). The sensors are located within a few millimeters of insulation and thus measure the wall temperature.

2.2. Optical emission spectroscopy

2.2.1. Equipment and experimental setups

Two spectrometers were used in the experiments: model AvaSpec-3648-RS and AvaSpec-ULS2048L from Avantes. The AvaSpec-3648-RS measures a spectrum from 496 nm to 1048 nm, and a detector consists of 3648 pixels, whereas the AvaSpec-ULS2048L can measure a spectrum from 250 nm to 1100 nm, and a detector consists of 2048 pixels. The wavelength range from 500 nm to 1000 nm was used for the analysis. Experiments aimed to measure the flame's radiation power, soot particles, and temperature. Radiation power could be determined by integrating intensities of all measured wavelengths. Temperature and soot particle measurements were based on grey body radiation.

The spectrometer continuously measured spectra, so when it finished one spectrum, it started recording another. For example, in a 30-minute session, approximately 4500 individual spectra were recorded, which means about 2.5 spectra per second.

During the open flame measurements, two different setups were used to install optical fiber, and one setup was used for the burner-heated furnace experiment (Table 1). At open flame measurements, optical fiber was installed from the flame at a 90° angle, and the burner-heated furnace test fiber was installed parallel to the burner.

2.2.2. Radiant heat and temperature analysis

The measured spectrum represents radiating power per wavelength. Therefore, relative radiation power could be determined by integrating intensities over the whole wavelength range. However, in this research, measurements covered the wavelength range from 500 nm to 1000 nm, representing only part of the spectrum. Therefore, the flame's relative intensity must be treated with caution, as molecular emissions outside the measured wavelength range could not be taken into account in the measurements.

Heat transfer can be defined as an energy transfer between two systems, and it can be separated into three mechanisms: radiant heat transfer, convection, and conduction [9]. As gases are good insulators, the role of conduction in the heat transfer of the flame to the heated object is negligible. Therefore, this section focuses on convection and radiant heat transfer.

Table 1
Open flame test setups (Test 1 and 2), and burner-heated furnace test setup (Test 3). Distances r and s are defined in Fig. 1.

Test	Spectrometer	Distance r [cm]	Distance s [cm]	Purpose of the experiment	Burner settings
1	AvaSpec-3648-RS	15	10	Heat radiation, temperature in different mixtures of NG and Hydrogen	15 kW, Lambda value 1.15
2	AvaSpec-ULS2048L	25	5,10,15,25,35	Spatial distribution of soot particles in different mixtures of NG and Hydrogen	30 kW, Lambda value 1.15
3	AvaSpec-3648-RS	0	270 parallel to the burner	Applicability test in burner-heated furnace	190 kW, Lambda value 1.05

Radiant heat transfer does not need a medium since energy is transferred by electromagnetic radiation. The background of radiant heat is thermal motion, which causes collisions of particles, leading to the excitation of electrons bound to atoms to a higher energy state. When an atom relaxes to the ground state, it emits a photon. As the temperature describes the motion of particles, it is easy to intuitively understand that higher temperature means higher radiative power of the object. However, radiative power also depends on the material of an object. For example, in the case of pure gases, excitations and relaxation of atoms and molecules are the main mechanisms to produce photons. For this reason, gases emit only certain wavelengths of electromagnetic radiation. In the case of solid materials, electrons can move more freely, which leads to a broader wavelength range. If the object is an ideal black, its radiation follows a black body curve [10]. Mathematical description of black body radiation is

$$B(\lambda,\ T) = \frac{2hc^2}{\lambda^5}\frac{1}{e^{hc/\lambda kT}-1} \tag{1}$$

where h is the Planck's constant, c is the speed of light, λ is the wavelength, k is the Boltzmann constant, and T is the temperature. The formula can be modified to approximate the radiance $L(\lambda,\ T)$ of real objects by adding emissivity ε to get a description of grey body radiation [11].

$$L(\lambda,\ T) = \varepsilon B(\lambda,\ T) \tag{2}$$

The previous equation assumes that ε is a constant whole temperature and wavelength range. This is not always accurate enough, and emissivity must be set as a function of temperature and wavelength when radiance can be described as

$$L(\lambda,\ T) = \varepsilon(\lambda,\ T)B(\lambda, T) \tag{3}$$

Considering the flame spectrum, typically, it is possible to find emission peaks from atoms and molecules as well as continuous curves of grey body radiation. The origin of atomic and molecular emission are hot exhaust gas components emitting characteristic emission peaks. The origin of the continuous part of the spectrum is typically soot particles, which act like a solid material and, therefore, produce continuous grey body radiation. As the spectrum represents spectral radiance per wavelength, the overall radiance (Fig. 2) is a combination of grey body radiation and molecular/atomic emissions.

Convective heat transfer refers to a mechanism where energy is

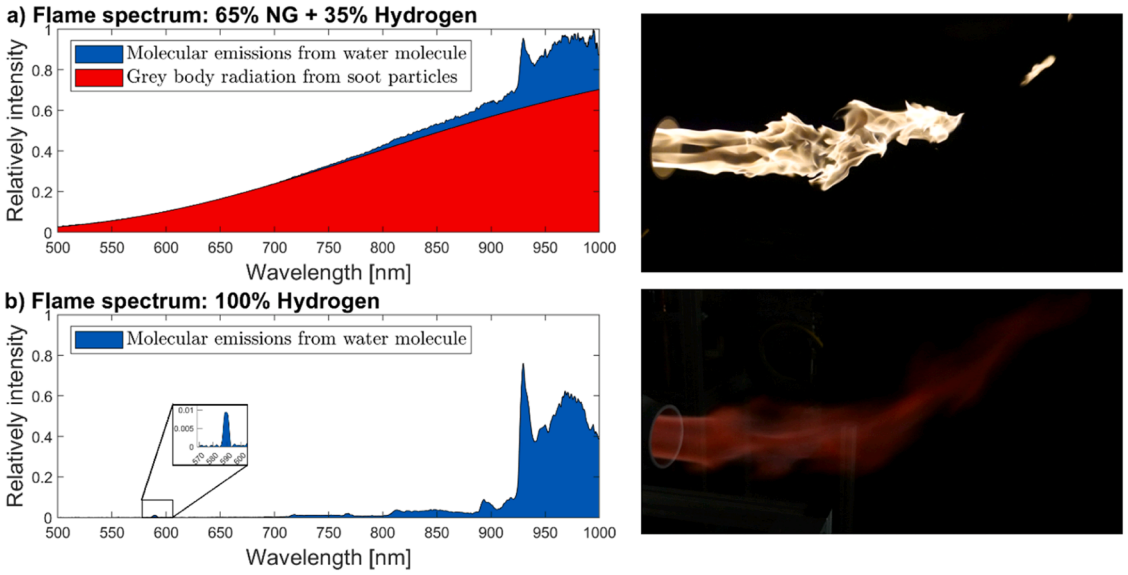

Fig. 2. The example spectra from a 15 kW open flame burner (Test 1), where a) is a spectrum from 65% NG and 35% hydrogen, and b) is a spectrum from 100% hydrogen. The percentage value indicates a share of power. The red area represents grey body radiation, and the blue represents molecular emissions from water molecules. Overall intensity in the measured wavelength range is a sum of blue and red areas. The 100% hydrogen flame spectrum consists only of molecular emissions, mainly from water molecules above 700 nm.

transported by fluid motion [9]. Macroscopic fluid motion can be separated into natural convection, where fluid motion is caused by density differences caused by temperature variation, and forced convection caused by external force. For example, gas burners use pressured oxidizers and flammable gas, which cause initial velocity for exhaust gases and force convection in a certain direction.

As soot is a solid material, it has a significant effect on radiant heat. The origin of soot is the carbon contained in hydrocarbon fuel. As the hydrogen fuel does not contain carbon, the hydrogen flame cannot produce soot. It follows that the hydrogen flame does not produce continuous grey body radiation, and the radiation of a hydrogen flame is mainly the result of molecular emissions, which leads to significantly lower overall radiation of hydrogen flame [12]. The logical consequence is that heat remains in the combustion products for a longer period of time, underscoring the importance of convective heat transfer. Fig. 2 represents an example of a natural gas-hydrogen mix and pure hydrogen flame. In the case of hydrogen, missing grey body radiation indicates missing soot particles, and a smaller overall area signifies a lower radiative power. The spectrum also explains why hydrogen flame is almost invisible to the human eye: emissions from water molecules are located in the wavelength area above what the eye can detect. Besides emissions from water molecules, a small emission peak can be seen at 589 nm, probably caused by sodium, which is present in small amounts in the air as an impurity and gives hydrogen flame a mild orange color [13].

In some cases, the flame temperature can also be determined from the spectra. OES temperature measurements are based on the same principle as the two color temperature measurements. Two color temperature measurements are based on comparing the intensities of two different wavelength ranges. The temperature can be approximated by using the equation [14]:

$$T = \left(\frac{1}{\lambda_2} - \frac{1}{\lambda_1}\right) \frac{hc/k}{\ln\left[\left(\frac{I_1}{I_2}\right)\left(\frac{\lambda_1}{\lambda_2}\right)^5\right]} \tag{4}$$

where h is Planck's constant, k is the Boltzmann constant, c is the speed of light, T is the temperature, λ is the wavelength, I is the intensity, and the lower index refers to selected wavelengths. The equation is derived from Wien's distribution law, which approximates Planck's law and is relatively accurate at temperatures below 5000 K [15]. This equation assumes that the radiation follows grey body radiation, which can lead to inaccuracies. For the open flame test, the emissivity of soot was considered in intensities I_1 and I_2. The wavelength-dependent emissivity was assumed to follow the equation [16]

$$\varepsilon_n(\lambda) = \frac{4\pi D}{\lambda} E_n(m) \tag{5}$$

where D is the diameter of soot particles, λ is the wavelength, and $E_n(m)$ is a function of a complex index of refraction, where lowercase n refers to Eqs. (6)-(8). In the literature, several experimental functions and theoretical background can be found for $E_n(m)$ [16]. Three experimental equations for $E_n(m)$ were chosen for comparison for open flame temperature measurements.

$$E_1(m) = 0.232 + 1254.6\lambda \tag{6}$$

$$E_2(m) = \frac{28.72}{6\pi} \lambda^{1-0.83} \tag{7}$$

$$E_3(m) = 1 \tag{8}$$

Emissivity is defined as a ratio of the actual radiation and the radiation of the ideal black body. Therefore, the intensity of the black body I_{BB} at a certain wavelength λ can be expressed as

$$I_{BB} = \frac{I}{\varepsilon(\lambda)} \tag{9}$$

To improve the accuracy of Eq. 4, the measured intensities I_1 and I_2 can be replaced by the calculated intensities of the blackbodies I_{BB1} and I_{BB2}. As Eq. 4 concerns ratios of intensities of two wavelengths, the diameter of soot particles can be canceled from the equation. In the case of the burner-heated furnace, the emissivity of the wall was unknown, so the emissivity was assumed to be constant over the measured wavelength range.

As the OES measures spectra, the intensities used for temperature measurements are not limited to two wavelengths. In this case, five wavelengths were used to create nine wavelength pairs for the temperature calculations (Table 2). As the spectrum is a combination of atomic or molecular emissions and grey body radiation, the wavelengths must be chosen so that there are no atomic or molecular emissions in the

Table 2
Wavelengths used for temperature measurements in the case of open flame and furnace.

	Open flame (nm)	Furnace (nm)
λ_1	550	600
λ_2	600	625
λ_3	650	650
λ_4	690	675
λ_5	700	700
Pairs	(λ_1,λ_2); (λ_1,λ_3); (λ_1,λ_4); (λ_1,λ_5); (λ_2,λ_3); (λ_2,λ_4); (λ_2,λ_5); (λ_3,λ_4); (λ_3,λ_5)	

selected wavelengths, which excludes wavelengths above 730 nm. Also, the wavelengths below 550 nm were excluded because radiation in flame temperature is relatively low in lower wavelengths, and stray light and dark current can interfere with measurements. Each pair of wavelengths gives an individual temperature value. The measurement result was considered the average, and the standard deviation of the individual measurements was defined as the error limits.

2.2.3. Spectral analysis

The spectrometer is a device that measures light intensity with respect to the wavelength. In practice, light comes into the spectrometer in a small slit, and after the slit, light hits a grating which reflects different wavelengths to different angles. Light is reflected to the detector, consisting of a row of pixels; every pixel represents some wavelength distribution. As the detector efficiency depends on wavelength, there may be efficiency differences between pixels and differences in how different wavelengths pass the optical fiber; the spectrometer must be calibrated. In this case, calibration was established with the SLS 201 stabilized light source [17].

Most of the spectrometer settings used in measurements were preset in the factory. However, exposure time could be adjusted. The spectrometer software observed the amount of light during measurements and automatically adjusted exposure time by light intensity. For this reason, exposure time varies between recorded spectra, and spectra must be normalized to match each other. As the detector type of both spectrometers is a charge-coupled device (CCD), it can be approximated that the detector's sensitivity to detecting photons is linear. Spectra could be normalized to correspond to some specific exposure time t_c to multiply the intensities of spectra by the factor $\frac{t_c}{t_E}$ where t_E is an exposure time of individual spectra.

Besides the signal from the flame, spectra consist of stray light, read noise, and dark current. Read noise can be assumed to be zero for the used spectrometer; therefore, the signal-to-noise ratio can be described as [18]

$$\frac{S}{N} = \frac{I_s}{\sqrt{I_s + 2I_b}}\sqrt{t} \tag{10}$$

where I_s is the flux of the light source (unit: photos/second), I_b is the flux of the background, including dark current and stray light, and t is the exposure time. The equation shows that increasing exposure times increases the signal-to-noise ratio by a factor of $\sqrt{t}$. Combining multiple spectra corresponds to increased exposure time as the read noise is insignificant. For this reason, five spectra were combined for analysis.

Another way to reduce noise in spectra is to combine the intensities of pixels. In this case, spectra were processed so that new spectra were created from raw spectra, where each pixel was the average value of the pixel itself and the six nearest pixels. This procedure significantly reduces the variation in temperature measurements caused by random noise in the spectra.

2.3. Calculation of adiabatic flame temperature

The adiabatic flame temperature was calculated using the SIM module of HSC Chemistry 10 (ver. 10.4.0.1). The studied burners were modeled as a *pyro unit*, with burner gas and air as the input flows and off-gas as the output flows. The pyro unit is set to *equilibrium mode* to calculate the chemical equilibrium of the input flows at a given temperature and pressure. In HSC Sim, the chemical equilibrium is calculated using the Gibbs energy minimization method proposed by White et al [19]. In this work, the off-gas temperature was adjusted using an embedded tangential control algorithm to attain adiabatic conditions, i.e., equal energy flows into and from the reactor. The pressure was assumed to correspond to atmospheric pressure (1 atm = 101,325 Pa) and the residual error for energy balance was set to $1 \bullet 10^{-10}$ kW. Table 3 shows the temperatures, pressures, and compositions of the burner gas and air employed in the simulations. In the model, the volumetric flows of the burner gas and air were set to correspond to their measured values to achieve the same air/fuel ratios as those employed in the experiments.

3. Results and discussion

3.1. Open flame

In the open flame experiments, the composition of the burner gas was changed from 100% natural gas to 100% hydrogen by increasing the hydrogen content stepwise, as shown in Fig. 3. As mentioned in Section 2.2.2, the soot formed in the flames significantly affects the heat radiated by the flame. For this reason, the relative amount of thermal radiation with different mixture ratios of hydrogen and natural gas was measured from the spectra. The method could not measure the absolute amount of thermal radiation, but the relative differences between different mixture ratios could be measured in the used wavelength range.

Based on the measurements, it can be observed that when hydrogen is added to a natural gas flame, the thermal radiation rises, reaching a peak when the hydrogen's share of the power is about 5% in test 1 (Fig. 3) and 16% in test 2 (Fig. 4). After this, when hydrogen increases, the radiation power drops radically (Fig. 3). The decrease in radiant power with large amounts of hydrogen is likely the result of a decrease in the amount of carbon in the fuel and, thus, less soot formation. The research also tried to discover which phenomenon caused the increase in the radiation power of small hydrogen shares. Two possible explanations were envisaged: 1) a small amount of hydrogen changes the combustion reaction, increasing the amount of soot, and 2) adding

Table 3
Properties of the burner gas and fuel.

Gas	Natural gas	Air
Temperature [°C]	25	25
Pressure [Pa]	101,325	101,325
Species	Composition [vol-%]	Composition [vol-%]
Ar(g)		0.934
C_2H_6(g)	6.93	
C_3H_8(g)	1.25	
C_4H_{10}(1barg)	0.35	
CH_4(g)	88.71	
CH_4(g)		0.000187
CO(g)	0	
CO_2(g)	1.94	0.0417
CO_2(g)		
H_2(g)	0	
H_2O(g)	0	
He(g)		0.000524
Kr(g)		0.000114
N_2(g)	0.82	78.075657
Ne(g)		0.001818
O_2(g)	0	20.946
Total	100	100

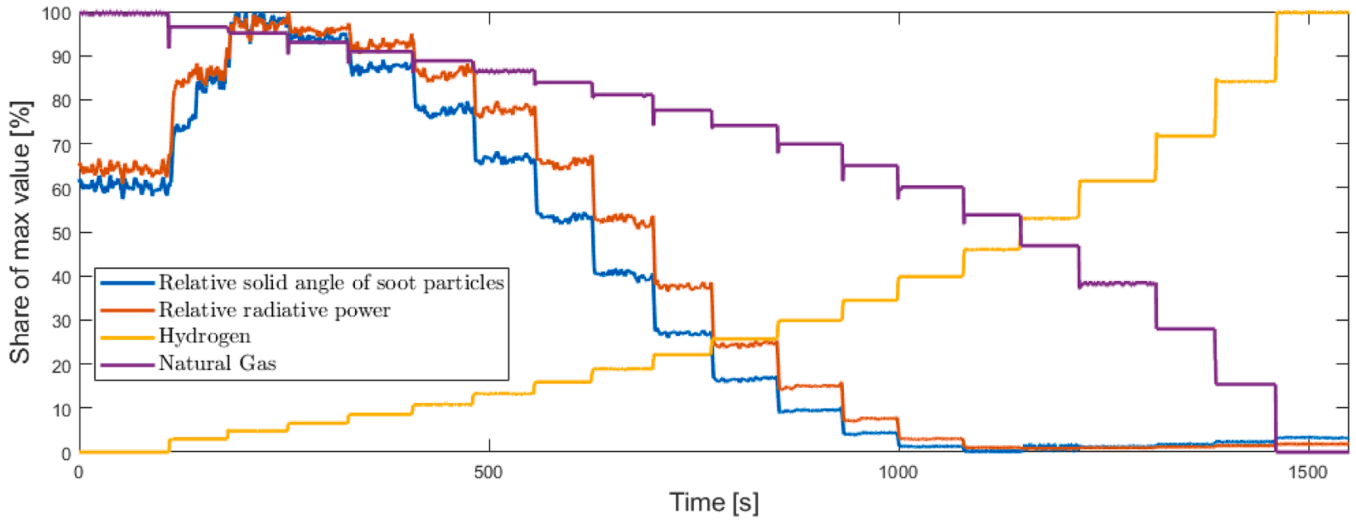

Fig. 3. Relative radiative power in 500–1000 nm wavelength range and relative solid angle of soot particles in different mixtures of NG and Hydrogen (Test 1).

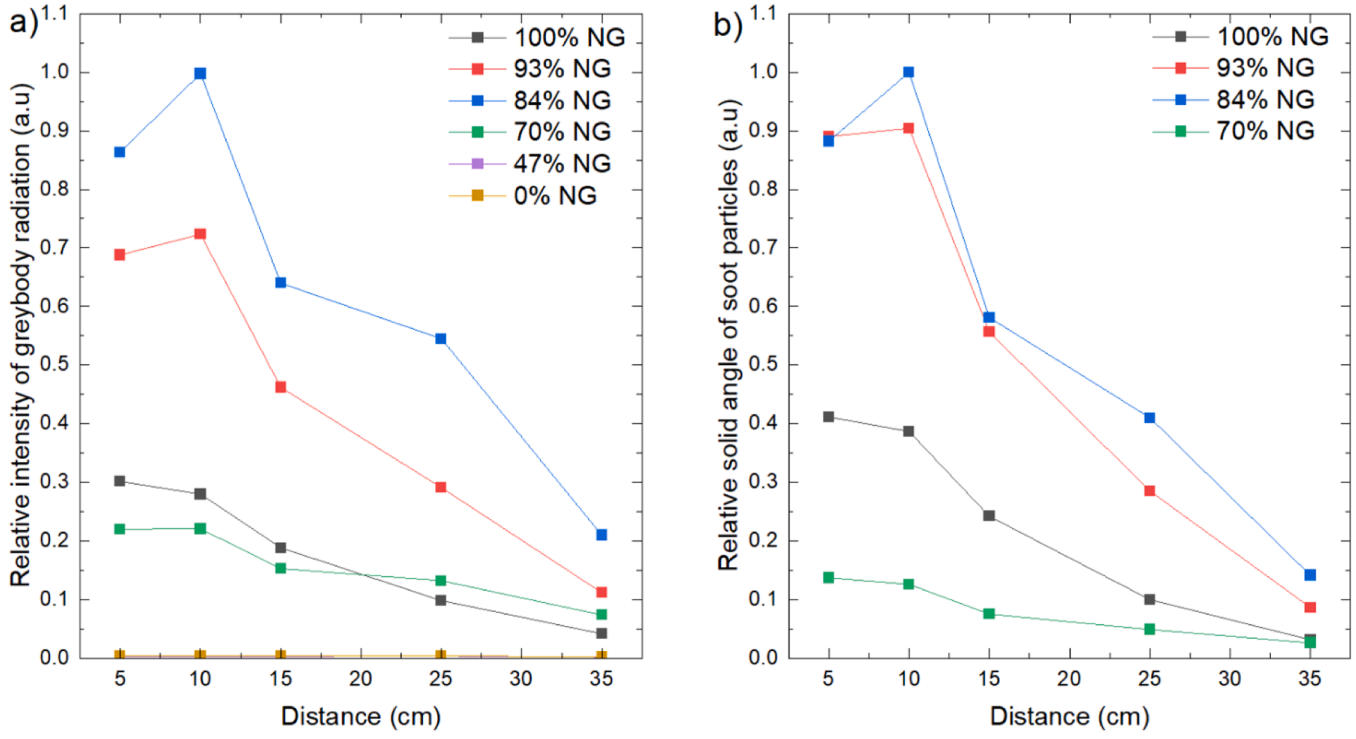

Fig. 4. a) Grey body radiation of the flame by distance from the nozzle (Test 2), and b) relative solid angle of soot particles.

hydrogen increases the temperature, leading to higher radiant heat. To investigate this question, a part of the spectra, from 520 nm to 730 nm, was isolated to consist only of continuous grey body radiation without significant molecular or atomic emissions. The intensity of this part was correlated with a temperature-dependent coefficient so that the radiating solid angle could be determined. In practice, this procedure eliminates the effect of temperature of the radiation of soot particles, resulting in a relative solid angle of soot particles in the view cone of the optical fiber. The solid angle of soot particles is proportional to the amount of soot particles, assuming $V_s \ll V_f$, where V_s on overall volume of soot particles and V_f is volume of the flame, and the size distribution of soot particles are the same in all fuel mixtures. Coefficient factors were calculated by measuring temperature from spectra. For this reason, the coefficient factor is not accurate when radiation from soot particles is very low, over 40% share of hydrogen. However, this method cannot measure the absolute amount or size distribution of soot particles, but the relative solid angle of soot particles could be measured. Fig. 3 shows the flame's relative radiation power and relative solid angle of soot particles by share of natural gas and hydrogen. Relative radiation power represents a sum of all measured intensities in the 500–1000 nm wavelength range. Based on test 1, the solid angle of soot particles reaches the maximum level of about 5% share of the hydrogen and keeps a higher level as pure natural gas flame up to 15% share of hydrogen. Similar observations can be found in the literature [20], However, soot studies generally show that hydrogen reduces soot loading monotonically [21]. A possible explanation for the contradiction between this study and other studies is that the previous assumption about the size distribution of soot particles is not correct. Hydrogen may limit the

growth of soot particles [22], which may result in more small soot particles and, thus, more radiating surface area. The difference between test 1 and test 2 probably results from different power settings of the burner. This phenomenon could be utilized in industrial applications if there is a need for higher radiative heat transfer. In applications with high proportions of hydrogen, lower radiative heat transfer and higher convective heat transfer should be considered.

As mentioned before, measurements cover a 500–1000 nm wavelength area and do not take into account molecular emissions from the infrared area, which causes inaccuracies in radiative power measurements. The results can probably be improved by combining spectral measurements with line-by-line absorption coefficient calculations [23].

In the open flame experiment, spectra were recorded perpendicular to the flame. Flame properties vary in different parts of the flame; therefore, measurements were also established at different distances from the nozzle. The burner used in experiments was designed to burn different mixtures of NG and hydrogen effectively, and it should not produce soot. However, spectral measurements show a continuous spectral curve, typical for solid materials. As the continuous curve disappears when using hydrogen, it is apparent carbon produces soot particles that create spectral features typical of solid surfaces. The effects of soot particles on a spectrum can also be found in the literature [12]. The explanation for the contradiction between a non-sooting burner and soot in the flame is most probably that hydrocarbon flames produce soot, but the soot burns off as it propagates through the flame. Measurements were established at different distances from the nozzle to study this aspect.

The overall intensity of the grey body radiation indicates a total solid angle of soot particles at a certain temperature in the view cone of the optical fiber.

Fig. 4 shows the evolution of the grey body radiation of the flame with distance from the nozzle. Decreasing intensity can be interpreted as reducing the number of soot particles. By extrapolating the curves, the intensity of grey body radiation decreases to zero at about 40 cm from the nozzle, corresponding to the empiric evaluation of visible flame length.

The flame temperature was also measured in test 1 from spectra in different mixtures of NG and Hydrogen, as shown in Fig. 5. Since the measurements are based on grey body radiation caused by soot, the temperature could be measured only when hydrogen content was lower than 46% of the maximum value. With higher proportions of hydrogen, the grey body radiation was too low to provide sufficient signal for temperature measurements. Interestingly, the temperature reaches the lowest value when the share of hydrogen is about 5%. This is probably related to the solid angle of soot particles. Fig. 3 shows that the maximum solid angle of soot particles is also in the 5 % share of hydrogen. The greater area of soot particles leads to higher heat radiation, leading to more rapid cooling of combustion products.

Lower heat radiation of hydrogen flame may also affect the formation of *NOx* compounds in a hydrogen flame. The higher *NOx* formation of a hydrogen flame is typically explained by the higher temperature of the hydrogen flame [24]. However, this may be only a partial explanation for higher *NOx* formation. Thermal *NO* formation mechanisms are the dominant route for *NOx* emissions in gas burners. The reaction is relatively slow and highly dependent on temperature [25]. The lower thermal radiation causes the heat to remain longer in the combustion gases, allowing more time for the NO molecule to get closer to chemical equilibrium. However, this hypothesis cannot be verified by the data of this research.

Theoretical values of temperature are shown in Fig. 5. The value indicates adiabatic flame temperature and gives the maximum value for flame temperature; the actual temperature must be lower than the theoretical temperature. The differences between theoretical and measured values also follow the relative solid angle of soot particles. This indicates that flames producing more soot radiate more energy, leading to lower flame temperature. Several options for soot emissivity can be found in the literature [16]. Fig. 6 compares the effect of different emissivity equations for temperature measurements. Table 4 shows an example of the numerical values of the temperatures with different emissivity functions.

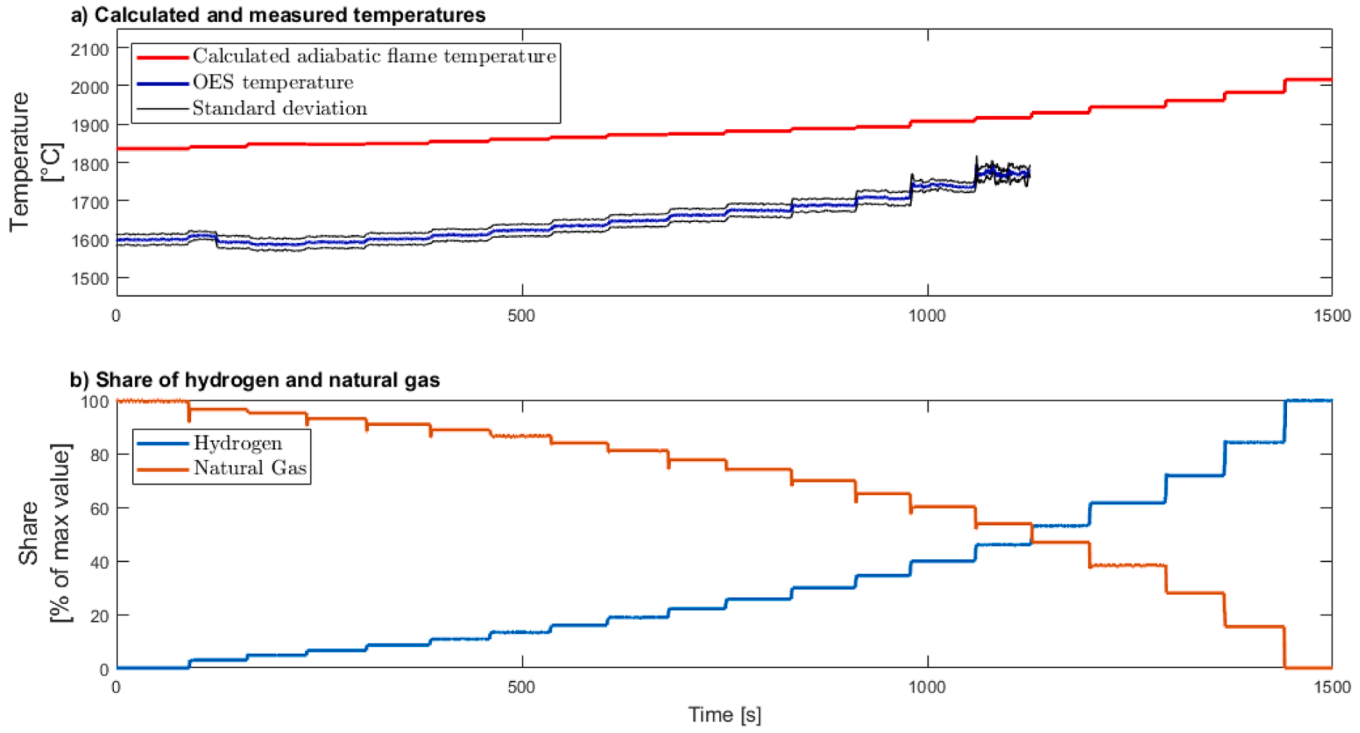

Fig. 5. The flame temperature in different shares of hydrogen and natural gas for Test 1. Temperature could be measured up to 46 % of hydrogen share. In higher shares of hydrogen, the signal from grey body radiation was too low for analysis. The theoretical value of temperature indicates adiabatic flame temperature for used gas mixtures. Emissivity is calculated by using the Eqs. (5) and (6).

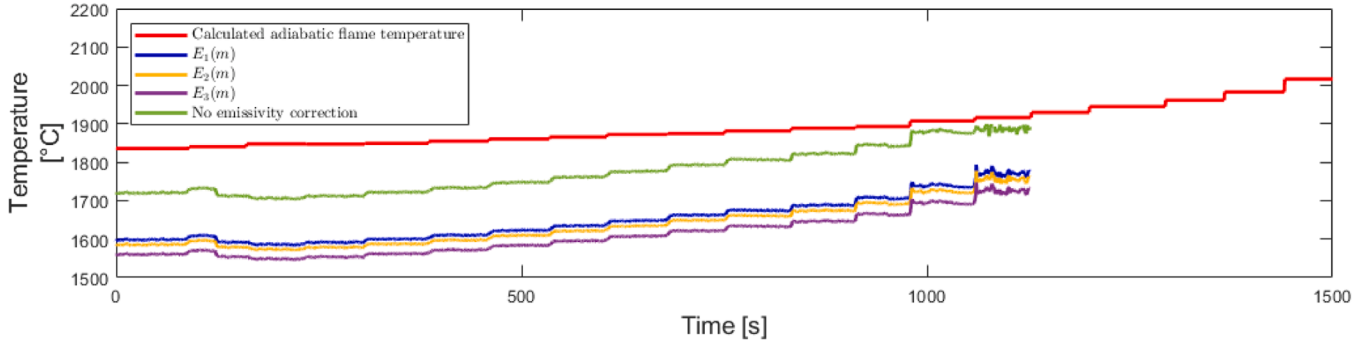

Fig. 6. The comparison of temperature values between different refractive index functions. $E_n(m)$ refers to the Eqs. (6)-(8). "No emissivity correction" -curve indicates temperature if the emissivity of soot particles does not depend on wavelength and the radiation follows the grey body radiation curve.

Table 4
An example of values of temperature and standard deviation of different emissivity functions. The temperature describes a flame temperature of 11% hydrogen and 89% natural gas content.

Emissivity function	Temperature [°C]	Standard deviation [°C]
$\varepsilon_1(\lambda)$	1610	16
$\varepsilon_2(\lambda)$	1597	18
$\varepsilon_3(\lambda)$	1572	19
Without emissivity	1734	13

Based on this research, it cannot be said for certain which equation describing emissivity is the most appropriate, as the actual temperature of the flame is unknown. However, without considering emissivity, the temperatures are very close to the calculated theoretical values, which indicates that these temperature values are too high. Emissivity function $\varepsilon_3(\lambda)$ does not take into account the refraction index of the soot particles, and it can be understood as a simplified version of $\varepsilon_1(\lambda)$ and $\varepsilon_2(\lambda)$. The temperature values calculated by all functions react similarly to composition changes, indicating that they all can be used to monitor relative temperature changes. Functions $\varepsilon_1(\lambda)$ and $\varepsilon_2(\lambda)$ are the more sophisticated functions and probably more accurate.

3.2. Burner-heated furnace

One of the research goals was to investigate the applicability of the OES for temperature measurement for industrial furnaces. Therefore, the temperature was measured from spectra in the burner-heated furnace, and OES temperature results were compared with data from thermocouples. Open flame analytics can be used to understand the principles of flame properties, but the situation is more complex in furnaces. The burner produces combustion gases at a relatively high speed, so the forced convection of the burner is responsible for a large part of the heat transfer. As a result of convection and thermal radiation, the heat is transferred to the furnace's walls, which start emitting thermal radiation. When measuring flame spectra in a furnace, there is always a hot wall behind the flame. Therefore, spectra are a combination of radiation from the flame and wall, making flame analysis more complicated. Furthermore, a good view into the furnace and the flame are prerequisites for OES measurements.

OES spectra were measured from the opposite side of the furnace so that the flame, burner, and part of the wall were at the view cone of optical fiber. As expected, spectrographic differences between different gas mixtures were much more minor than in open flame experiments, which indicates that radiation from furnace walls dominates spectra. Fig. 7 shows measured spectra of 100% NG and 100% hydrogen. The most notable difference is higher water emissions (920–1000 nm) at

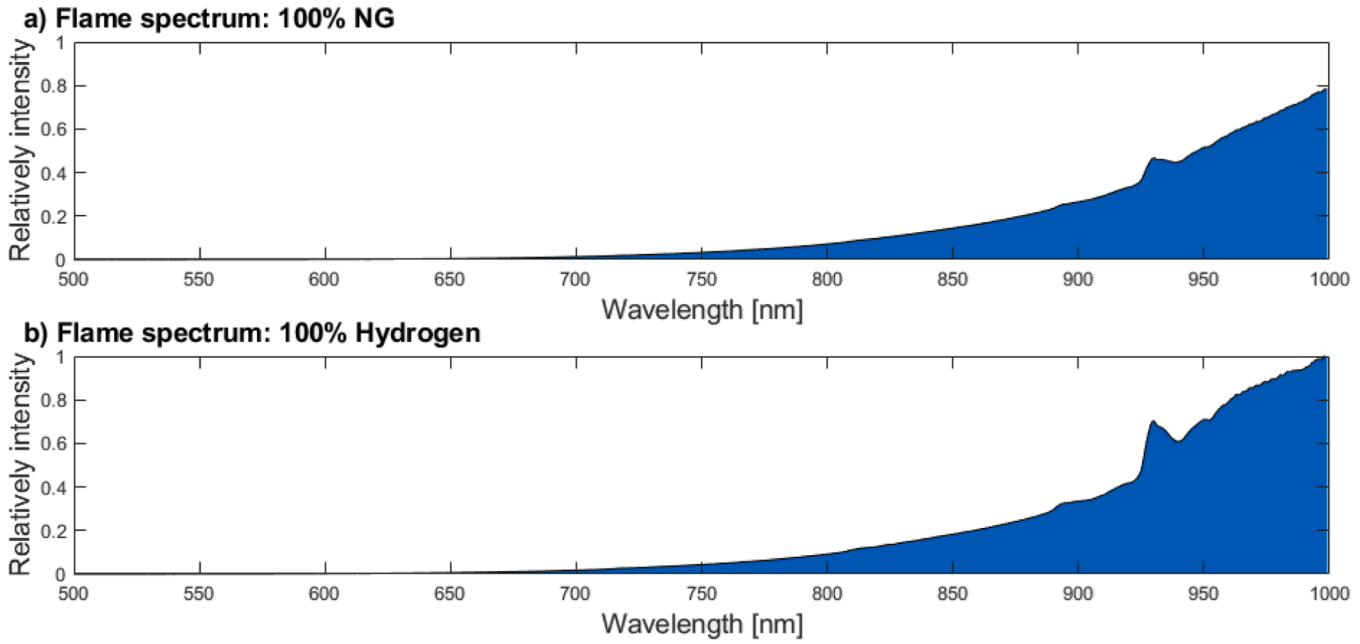

Fig. 7. Spectra from the burner-heated furnace at a) 100% natural gas, and b) 100% hydrogen.

100% hydrogen. The spectra are normalized to match each other to show the intensity difference.

As the grey body radiation-like curve exists in all gas mixtures, the temperature was measured from spectra. Fig. 8 shows the results of temperature measurements, including OES results and temperature sensors T1 and T8 (Fig. 1).

The temperature values correspond relatively accurately with data from thermocouples on furnace walls. This also indicates that radiation from the walls dominates spectra strongly, and the measured temperature is rather the wall's temperature than the flame's. As a result, the applicability of OES for flame analysis in the 500–1000 nm wavelength range is questionable in furnaces. However, OES provides temperature values that correspond with temperature sensors' values on the furnace wall. The used wavelength range is probably not optimal for flame analysis in furnaces. The most intermediate molecules that can be expected to form when natural gas or hydrogen is burned are located in the shorter wavelength range, as used in this study. Also, radiation from the furnace walls can be expected to be less intensive in shorter wavelengths, meaning that measurements in ultraviolet can provide a better signal from the flame itself.

3.3. Analyzing time

All the analyses were done after the measurements, but one of the secondary goals of the research was to determine if it is possible to use OES for real-time analysis. Processing time may limit the use of OES online measurements if spectrometers collect more spectra than a computer can process. Therefore, the analysis time of the measurement session was measured. Table 5 shows the time spent on analysis. The time consists of calibration, summing, reducing the noise of spectra, and analysis of relative radiation power and temperature. If the time used to analyze the measurements is shorter than the time used for the measurements, it can be concluded that the processing speed does not limit the real-time analysis. The results show that the analysis time is significantly shorter than the time of the measurement session.

4. Conclusions

The study concludes that the OES method is suitable for measuring thermal radiation from burners. It should be noted that the spectrometer covered the wavelength range of 500–1000 nm, which represents only part of the overall thermal radiation. However, observations supported empirical experiences and the literature [12] on hydrogen flame's thermal radiation. The actual radiation intensity of the flame was not measured in this study, and the measured value is relative. Interpretation of the spectra gave a good overall picture of why there is a difference between the thermal radiation of a hydrogen flame and a natural gas flame. The carbon in natural gas produces soot particles, which produce broadband grey body radiation and increase the flame's total radiation. As the hydrogen fuel does not contain hydrocarbons that could form soot, the spectrum of the hydrogen flame in this wavelength range consists only of molecular emissions from water molecules, leading to lower overall radiation. When comparing different mixture ratios of hydrogen and natural gas, increasing the hydrogen content initially increased the amount of thermal radiation, reaching a peak value when hydrogen accounted for about 5% of the power, after which the radiation power began to drop sharply. Similar observations in the literature [20] indicate that the observed phenomenon is universal. This observation should be considered when designing hydrogen-powered burner processes. The present study also gives a possible explanation as to why soot can be detected from the flame even when the burner is designed for non-sooting combustion. In short, soot forms in the flame, but burns off as it propagates through the flame.

The flame temperature could be measured at high concentrations of natural gas. In the context of this study, the temperature could not be verified by other methods, so the absolute error of the result could not be determined. However, the relative temperature change was as expected, and all emissivity functions show similar relative temperature changes, which indicates that the method can probably be used reliably to monitor temperature changes. Reference measurements would be needed to obtain an absolute result. In this case, the temperature measurement was based on the grey body radiation. Therefore, the

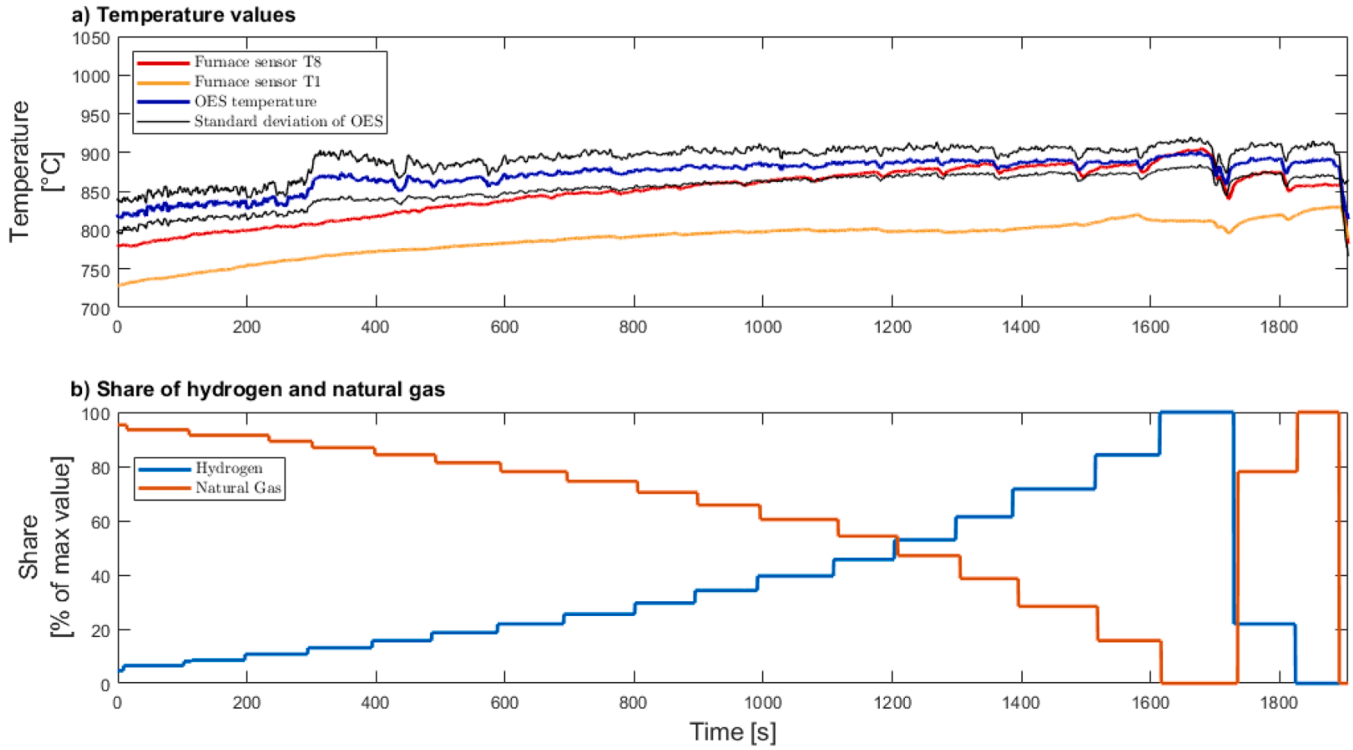

Fig. 8. Temperature measurements of 190 kW furnace. The graph includes OES data and data from temperature sensors T1 and T8 (Test 3).

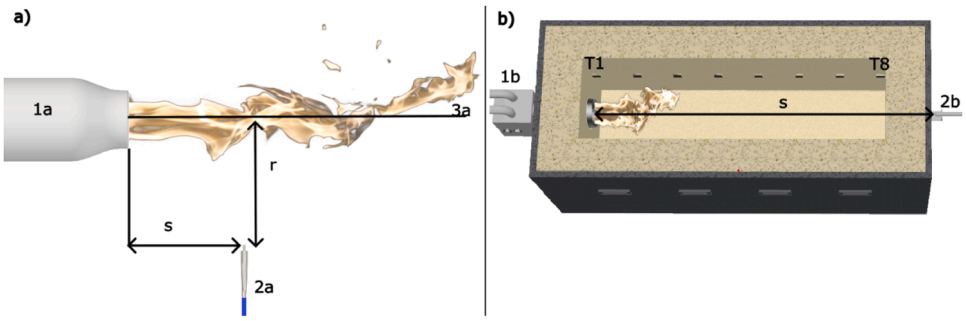

Fig. 1. Schematic representation of the experimental setups: a) open flame test setup, b) burner-heated furnace. In the open flame test setup, 1a is the burner, 2a is the measuring head, and 3a is the center line of the burner. The symbol s represents the optical fiber's distance from the burner's nozzle, and r represents the distance from the center line of the burner. In the burner-heated furnace, 1b is the burner, and the 2b is the measuring head. The symbol s represents the measuring head's distance from the burner nozzle. Symbols T1 and T8 represent temperature sensors. Numerical values for s and r can be found in Table 1.

Table 5
Processing times of spectra.

Processor and memory	Analyze time [s]	Amount of spectra	Session time [min]	Measured spectra per second	Analyzed spectra per second
i5–10210U, 16 GB	37.5	4534	31	2.4	121
I5–13600K, 32GB	11	4534	31	2.4	412

temperature could only be determined when the natural gas share was high enough to produce observable grey body radiation. The limit value for temperature measurements was 46% share of hydrogen. This value is likely to depend on the design of the burner and the air-fuel equivalence ratio. In the burner-heated furnace tests, the thermal radiation from the furnace walls complicated the flame analysis. The optical fiber measures all the radiation entering it, and in a furnace, it is impossible to position the sensor so that it does not also point to the furnace wall. The radiation from the furnace wall dominated the spectrum, so the radiation power of the flame could not be measured directly. On the other hand, the temperature measurements from the spectral measurements performed in the furnace corresponded well with the results from the furnace's temperature sensors. Hence, the temperatures described the wall's temperature opposite the sensor, rather than the flame's temperature. Wall temperatures are probably more reasonable to measure with thermocouples, but OES is probably also suitable for measuring the surface temperature of a heated object, for example, a metal slab. A spectrometer capable of measuring light in the ultraviolet range is probably more suitable for flame analysis in furnaces, as it would allow measurements of intermediate molecules relevant to NG and hydrogen combustion processes.

Novelty and significance

Optical spectroscopy has had a significant historical role in the development of physics, chemistry, and astronomy. Historically, the slowness of data analysis has hindered the use of optical spectroscopy in real-time applications. Over the last decade, optical spectroscopy has been studied for monitoring electric furnaces, and the method has proven valuable. This research extends the use of optical spectroscopy to the analysis of combustion processes.

CRediT authorship contribution statement

Arto Rautioaho: Writing – original draft, Software, Methodology, Investigation, Data curation. **Henri Pauna:** Writing – review & editing, Supervision, Project administration, Methodology, Funding acquisition, Conceptualization. **Mikko Jokinen:** Resources, Investigation. **Oskari Seppälä:** Resources, Investigation. **Elsa Busson:** Writing – review & editing, Resources, Investigation. **Lukas Sankowski:** Writing – review & editing, Resources, Investigation. **Ville-Valtteri Visuri:** Writing – review & editing, Writing – original draft, Supervision, Resources. **Timo Fabritius:** Writing – review & editing, Supervision.

Declaration of competing interest

The authors declare that they have no known competing financial interests or personal relationships that could have appeared to influence the work reported in this paper.

Acknowledgements

This work was supported by the European Union's Horizon EU research and innovation programme under grant agreement no. 101091456 for the HyInHeat project, the Research Council of Finland under the H2Future grant no. 352788, JustH2Transit grant no. 358422, post-doctoral research grant no. 349402 (Henri Pauna), and academy research fellow grant no. 356439 (Ville-Valtteri Visuri).

Data availability

Data will be made available on request.

References

[1] Holappa L. A general vision for reduction of energy consumption and CO2 emissions from the steel industry. Metals 2020;10(9). https://doi.org/10.3390/met10091117.
[2] Airaksinen S, Haapakangas J, Laukka A, E.-P. Heikkinen E-P, Fabritius T. Oxide scale formation of stainless steels with different heating methods – Effect of hydrogen as fuel. Steel Res. Int. 2024;95(1). https://doi.org/10.1002/srin.202300334.
[3] Dudley W. Methods of experimental physics; v13. Manhattan, Kansas: Academic Press; 1976.
[4] Hearnshaw J. Astronomical spectrographs and their history, Cambridge; 2009.
[5] Brand J. Lines of light: the sources of dispersive spectroscopy, 1800-1930. 2017. London.
[6] Pauna H, Aula M, Kaukonen S, Huttula M, Fabritius T. Optical emission spectroscopy as a tool for process control of steelmaking burner. In: 8th International Congress on the Science and Technology of Steelmaking; 2022. https://doi.org/10.33313/531/022.
[7] Aula M, Leppänen A, Roininen J, Heikkinen E-P, Vallo K, Fabritius T, Huttula M. Characterization of process conditions in industrial stainless steelmaking electric arc furnace using optical emission spectrum measurements. Metall. Mater. Trans. B 2014;45:839–49. https://doi.org/10.1007/s11663-014-0032-0.
[8] Pauna H, Aula M, Seehausen J, Klung J-S, Huttula M, Fabritius T. Industrial ladle furnace slag composition analysis with optical emissions from the arc. ISIJ Int 2020;60(9):1985–92. https://doi.org/10.2355/isijinternational.ISIJINT-2019-676.
[9] Incropera F, Dewitt D, Bergman T, Lavine A. Fundamentals of heat and mass transfer. John Wiley & Sons; 2007.
[10] Young HD, Freedman RA, Ford LA. Sears and zemansky's university physics with modern physics. Pearson; 2014.

[11] Weiser V, Eisenreich N. Fast emission spectroscopy for a better understanding of pyrotechnic combustion behavior. Propellants Explos. Pyrotech 2005;30:67–78. https://doi.org/10.1002/prep.200400087.
[12] Yin Y, Medwell PR, Gee AJ, Foo KK, Dally BB. Fundamental insights into the effect of blending hydrogen flames with sooting biofuels. Fuel 2023:331. https://doi.org/10.1016/j.fuel.2022.125618.
[13] Arens EE, Youngquist RC, Starr SO. Intensity calibrated hydrogen flame spectrum. Int J Hydrogen Energy 2014;39(17):9545–51. https://doi.org/10.1016/j.ijhydene.2014.04.043.
[14] Aula M, Mäkinen A, Leppänen A, Huttula M, Fabritius T. Optical emission analysis of slag surface conditions and furnace atmosphere during different process stages in electric arc furnace (EAF). ISIJ Int 2015;55:1702–10. https://doi.org/10.2355/isijinternational.ISIJINT-2015-042.
[15] Pauna H, Aula M, Seehausen J, Klung J-S, Huttula M, Fabritius T. Optical emission spectroscopy as an online analysis method in industrial electric arc furnaces. Steel Res. Int. 2020;91(11). https://doi.org/10.1002/srin.202000051.
[16] Goulay F, Schrader P, Michelsen H. Effect of the wavelength dependence of the emissivity on inferred soot temperatures measured by spectrally resolved laser-induced incandescence. Appl. Phys. B: Lasers Opt 2010;100:655–63. https://doi.org/10.1007/s00340-010-4119-2.
[17] Thorlabs inc., "SLS201 - Stabilized Fiber-coupled light source," [Online]. Available: https://www.thorlabs.com/thorproduct.cfm?partnumber=SLS201. [Accessed 11 3 2025].
[18] Romanishin W. An introduction to astronomical photometry using CCDs. University of Oklahoma; 2006.
[19] White WB, Johnson SM, G B. Dantzig chemical equilibrium in complex mixtures. The Journal of Chemical Physics 1958;28(5):751–5. https://doi.org/10.1063/1.1744264.
[20] Cozzi F, Coghe A. Behavior of hydrogen-enriched non-premixed swirled natural gas flames. Int. J. Hydrogen Energy 2006;31(6):669–77. https://doi.org/10.1016/j.ijhydene.2005.05.013.
[21] Wang Y, Gu M, Zhu Y, Cao L, Zhu B, Wu J, et al. A review of the effects of hydrogen, carbon dioxide, and water vapor addition on soot formation in hydrocarbon flames. Int J Hydrogen Energy 2021;46(61):31400–27. https://doi.org/10.1016/j.ijhydene.2021.07.011.
[22] Sun Z, Dally B, Nathan G, Alwahabi Z. Effects of hydrogen and nitrogen on soot volume fraction, primary particle diameter and temperature in laminar ethylene/air diffusion flames. Combust Flame 2017;175:270–82. https://doi.org/10.1016/j.combustflame.2016.08.031.
[23] Fisher AS, Rani SL. A narrow band model based on the absorption coefficient and its application to the calculation of radiative transfer in one-dimensional enclosures. J. Quant. Spectrosc. Radiat. Transfer 2022:277. https://doi.org/10.1016/j.jqsrt.2021.107989.
[24] Skottene M, Rian KE. A study of NOx formation in hydrogen flames. Int. J. Hydrogen Energy 2007;32(15):3572–85. https://doi.org/10.1016/j.ijhydene.2007.02.038.
[25] Varatharajan K, Cheralathan M. Influence of fuel properties and composition on NOx emissions from biodiesel powered diesel engines: A review. Renewable Sustainable Energy Rev 2012;16(6):3702–10. https://doi.org/10.1016/j.rser.2012.03.056.